

Mobility and Saturation Velocity in Graphene on SiO₂

Vincent E. Dorgan,¹ Myung-Ho Bae,¹ and Eric Pop^{1,2,*}

¹*Dept. of Electrical and Computer Engineering, Micro and Nanotechnology Laboratory, University of Illinois, Urbana-Champaign, IL 61801, USA*

²*Beckman Institute, University of Illinois, Urbana-Champaign, IL 61801, USA*

We examine mobility and saturation velocity in graphene on SiO₂ above room temperature (300-500 K) and at high fields (~ 1 V/ μm). Data are analyzed with practical models including gated carriers, thermal generation, “puddle” charge, and Joule heating. Mobility displays a peak and saturation velocity decreases vs. carrier density. Both decrease slightly with temperature above 300 K. Saturation velocity is $>3 \times 10^7$ cm/s at low carrier density, and remains greater than in Si up to 1.2×10^{13} cm⁻² density. Transport appears primarily limited by the SiO₂ substrate, but results suggest intrinsic graphene saturation velocity could be more than twice that observed here.

*Contact: epop@illinois.edu

The excellent electrical and thermal properties of graphene hold great promise for applications in future integrated-circuit technology.¹ For instance, the electron and hole energy bands are symmetric,^{1,2} leading to equal and high electron and hole mobilities, unlike in typical semiconductors like Si, Ge or GaAs where hole mobility is lower. However, despite many measurements at low fields and low temperatures,³ surprisingly little data or models exist for transport in graphene at temperatures and high electric fields typical of modern transistors.

In this study we investigate mobility in the $T = 300\text{-}500$ K range and velocity saturation at fields $F \sim 1$ V/ μm in monolayer graphene on SiO₂, both as a function of carrier density. To analyze conductance data we introduce a simple model for the carrier density including the proper electrostatics and self-heating⁴ at high fields. We find that mobility peaks and saturation velocity decreases with respect to charge density. Both decrease with rising temperature in this range, and appear limited by the SiO₂ substrate. The relatively straightforward approach presented can be used for device simulations or applied to graphene on other substrates.

We fabricated four-probe graphene structures on SiO₂ with a highly doped Si substrate which also serves as the back-gate (Fig. 1a and supplementary material⁵). To obtain mobility and drift velocity from conductivity measurements, we model the carrier density including gate-induced (n_{cv}), thermally generated (n_{th}) carriers, electrostatic spatial inhomogeneity (n^*) and self-heating at high fields. Previous mobility estimates using only n_{cv} could lead to unphysically high mobility ($\mu \rightarrow \infty$) near the Dirac voltage ($V_G = V_0$) at the minimum conductivity point.

First, we note the gate voltage imposes a charge balance relationship as

$$n_{cv} = p - n = -C_{ox} V_{G0} / q, \quad (1)$$

where $C_{ox} = \epsilon_{ox}/t_{ox}$ is the capacitance per unit area (quantum capacitance may be neglected here^{6,7}), ϵ_{ox} is the dielectric constant of SiO₂, q is the elementary charge, and $V_{G0} = V_G - V_0$ is the gate voltage referenced to the minimum conductivity point. Next, we define an average Fermi level E_F such that $\eta = E_F/k_B T$, leading to the mass-action law:⁶

$$pn = n_{th}^2 \frac{\mathfrak{F}_1(\eta) \mathfrak{F}_1(-\eta)}{\mathfrak{F}_1^2(0)} \quad (2)$$

where $n_{th} = (\pi/6)(k_B T/\hbar v_F)^2$ is the thermal carrier density, $v_F \approx 10^8$ cm/s is the Fermi velocity, and $\mathfrak{F}_j(\eta)$ is the Fermi-Dirac integral, $\mathfrak{F}_1(0) = \pi^2/12$.

Next, we account for the spatial charge (“puddle”) inhomogeneity of graphene due to substrate impurities.^{8,9} The surface potential can be approximated⁷ as a periodic step function $\pm\Delta$ which implies that electron and hole puddles are equal in size near $V_G = V_0$. We relate the potential step to the measured width of the minimum conductivity plateau,^{5,10} which is given by the residual carrier puddle density (n^*) due to charged impurities in the SiO₂ (n_{imp}). We find $n^* \approx 0.297n_{imp} \approx 2.63 \times 10^{11} \text{ cm}^{-2}$ here,⁵ i.e. a surface potential variation $\Delta \approx 59 \text{ meV}$. This is similar to a previous study ($\sim 54 \text{ meV}$),⁷ and to scanning tunneling microscopy results ($\sim 77 \text{ meV}$).⁹ The surface potential inhomogeneity is equivalent to a Dirac voltage variation $\Delta V_0 = qn^*/C_{ox} \approx 3.66 \text{ V}$.

The total carrier density is determined by averaging Eqs. (1) and (2) for the regions of $\pm\Delta$, which can be solved numerically but does not yield an explicit expression. In order to simplify this, we note that at low charge density ($\eta \rightarrow 0$) the factor $\mathfrak{I}_1(\eta)\mathfrak{I}_1(-\eta)/\mathfrak{I}_1^2(0)$ in Eq. (2) approaches unity. At large $|V_{G0}|$ the gate-induced charge dominates, i.e. $n_{cv} \gg n_{th}$ when $\eta \gg 1$. Finally, we add a correction for the spatial charge inhomogeneity by noting that when this is taken into account the minimum carrier density is given by $n_0 = [(n^*/2)^2 + n_{th}^2]^{1/2}$. This results from averaging the regions of $\pm\Delta V_0$ near the Dirac point. Solving Eqs. (1) and (2) above with these approximations results in an *explicit* expression for the concentration of electrons and holes:

$$n, p \approx \frac{1}{2} \left[\pm n_{cv} + \sqrt{n_{cv}^2 + 4n_0^2} \right], \quad (3)$$

where the lower (upper) sign corresponds to electrons (holes). Equation (3) can be readily used in graphene device simulations, and is similar to a previous empirical formula.¹¹ Moreover, we note it properly reduces to the familiar $n = C_{ox}V_{G0}/q$ at high gate voltage, and $n = n_0$ (intrinsic puddle regime) at gate voltages near V_0 . Figure 1b displays the role of thermal and “puddle” corrections to the carrier density at 300 K and 500 K. These are particularly important near $V_{G0} = 0 \text{ V}$, when the total charge density relevant in transport ($n+p$) approaches a constant despite the charge neutrality condition imposed by the gate ($n-p = 0$). At higher temperatures ($k_B T \gg \Delta$) the spatial potential variations becomes less important due to thermal smearing and higher n_{th} .

Using the above, we obtain the mobility by measuring conductivity $\sigma = (L/W)I_{14}/V_{23}$ as a function of V_{G0} at low fields ($\sim 2 \text{ mV}/\mu\text{m}$). Mobility vs. carrier density is extracted as $\mu = \sigma/q(p+n)$ in Fig. 2a at various temperatures and $V_{G0} > 0$ ($n > p$), i.e. electron majority carriers.¹²

(the hole mobility and additional discussion is available in the supplement⁵). The mobility first increases, peaks at $\sim 4500 \text{ cm}^2/\text{V}\cdot\text{s}$ and $n \sim 2 \times 10^{12} \text{ cm}^{-2}$ (at 300 K), then decreases with carrier density. This suggests Coulomb scattering plays a role at low density, and phonon scattering at higher densities.⁷ Mobility decreases with rising $T > 300 \text{ K}$ for all carrier densities (Fig. 2b). This was also noted by Ref. 7, albeit in a lower temperature range.

We then took high-field drift velocity measurements, which pose challenges due to Joule heating and non-uniform potential (and carrier density) along the channel. To account for self-heating we calculate the average device temperature via its thermal resistance \mathcal{R}_{th} (Fig. 1a):²

$$\Delta T = T - T_0 \approx P(\mathcal{R}_B + \mathcal{R}_{ox} + \mathcal{R}_{Si}) \quad (4)$$

where $P = I_{14}V_{23}$, $\mathcal{R}_B = 1/(hA)$, $\mathcal{R}_{ox} = t_{ox}/(\kappa_{ox}A)$, and $\mathcal{R}_{Si} \approx 1/(2\kappa_{Si}A^{1/2})$ with $A = LW$ the area of the channel, $h \approx 10^8 \text{ Wm}^{-2}\text{K}^{-1}$ the thermal conductance of the graphene-SiO₂ boundary,¹³ κ_{ox} and κ_{Si} the thermal conductivities of SiO₂ and of the doped Si wafer.⁵ At 300 K for our geometry $\mathcal{R}_{th} \approx 10^4 \text{ K/W}$, or $\sim 2.8 \times 10^{-7} \text{ m}^2\text{K/W}$ per unit of device area. Of this, the thermal resistance of the 300 nm SiO₂ (\mathcal{R}_{ox}) accounts for $\sim 84\%$, the spreading thermal resistance into the Si wafer (\mathcal{R}_{Si}) $\sim 12\%$ and the thermal resistance of the graphene-SiO₂ boundary (\mathcal{R}_B) $\sim 4\%$. We note that the role of the latter two will be more pronounced for smaller devices on thinner oxides. The thermal model in Eq. (4) can be used when the sample dimensions are much greater than the SiO₂ thickness ($W, L \gg t_{ox}$) but much less than the Si wafer thickness.²

To minimize charge non-uniformity along the channel at high fields⁴ we bias the device at high $|V_G|$ and avoid ambipolar transport ($V_{GS} - V_0$ and $V_{GD} - V_0$ must have same sign).¹¹ We confirm this with finite-element simulations.^{4,5} The drift velocity is $v = I_{14}/(Wqn)$ where n is the average charge density between terminals 2 and 3, and the background temperature is set to $T_0 = 80 \text{ K}$ and 300 K . Due to self-heating ($T = T_0 + \Delta T$), the former enables measurements of saturation velocity (v_{sat}) close to room temperature and the latter above room temperature.

Figures 3a and 3b show the velocity-field relationship at the two background temperatures, indicating saturation tendency at fields $F > 1 \text{ V}/\mu\text{m}$. The drift velocity is fit by

$$v(F) = \frac{\mu_0 F}{\left[1 + (\mu_0 F / v_{sat})^m\right]^{1/m}}, \quad (5)$$

where μ_0 is the low-field mobility and the parameter $m = 2$ provides the best fit for all carrier densities and temperatures. To limit the role of self-heating, data was only fit up to $\Delta T \sim 200$ K (solid symbols).¹⁴ We also checked low-field $I-V_G$ characteristics were reproducible after each high bias measurement to ensure no sample degradation due to high field stress.¹⁴

Figure 3c shows extracted drift velocity vs. electron density (symbols) at $F = 2$ V/ μm , for the two back ground temperatures. To interpret the experimental high-field velocity, we compare it with an analytic model (dashed lines). This model approximates the high-field distribution with the two half-disks shown in the Fig. 3c inset, suggested by previous simulations.¹⁵ This assumes v_{sat} is limited by inelastic scattering with optical phonons (OP) and leads to the expression:¹⁶

$$v_{sat,0}(n, \omega_{OP}) = \frac{2}{\pi} \frac{\omega_{OP}}{\sqrt{\pi n}} \sqrt{1 - \frac{\omega_{OP}^2}{4\pi n v_F^2}}, \quad (6)$$

where $\hbar\omega_{OP}$ is the OP energy. In the limit of low carrier density this reduces to a constant, $v_{max} = (2/\pi)v_F \approx 6.3 \times 10^7$ cm/s (six times higher than v_{sat} in Si) and at high carrier density it scales as $v_{sat} = (2/\pi)\omega_{OP}/(\pi n)^{1/2}$, dependent both on the OP energy and the carrier density.

We consider the limit of two dominant phonon mechanisms in Fig. 3c, $\hbar\omega_{OP} = 55$ meV (dashed, SiO₂ substrate OP¹⁷) and $\hbar\omega_{OP} = 160$ meV (dotted, graphene OP¹⁸). The model limited by SiO₂ phonons slightly underestimates v_{sat} , while the model with graphene OPs significantly overestimates the measured v_{sat} . This suggests that both phonons play a role in limiting the saturation velocity, but that substrate phonons are dominant for graphene on SiO₂. (we note that for device simulations the fit can be optimized using an intermediate value $\hbar\omega_{OP} = 78$ meV.) Nevertheless, v_{sat} is greater than in Si for charge densities $n < 1.2 \times 10^{13}$ cm⁻² and more than twice that of Si at $n < 4 \times 10^{12}$ cm⁻². With only the graphene OP ($\hbar\omega_{OP} = 160$ meV) the model suggests an upper limit for the “maximum” v_{sat} that could be expected in graphene. This intrinsic v_{sat} could be more than twice as high as that measured here on SiO₂ and between two to six times higher than in Si for the charge density range considered here.

Finally, we note the data suggest a temperature dependence of v_{sat} which has not yet been included. To understand this, we recall the OP scattering rate is proportional to $(N_{OP} + 1)$, where $N_{OP} = 1/[\exp(\hbar\omega_{OP}/k_B T) - 1]$ is the phonon occupation.¹⁹ This suggests a temperature dependence qualitatively similar to that in Si.²⁰

$$v_{sat}(n, \omega_{OP}, T) = \frac{v_{sat,0}}{N_{OP} + 1} \quad (7)$$

where $v_{sat,0}$ is defined above. This model yields a $\sim 20\%$ change in v_{sat} between $T = 280$ K and 500 K if the SiO_2 phonon is dominant, and a $\sim 2\%$ change if the graphene OP is dominant. The data in Fig. 3c show much closer agreement with the former, once again indicating the strong effect of the SiO_2 in limiting graphene transport.

In summary, we examined mobility and saturation velocity in graphene on SiO_2 from conductivity measurements, accounting for electrostatic and temperature effects. This work falls in the $T > 300$ K and high field $F > 1$ V/ μm regime, where little experimental data exists. Both data and models point to the role of the SiO_2 substrate in limiting graphene transport. The models presented are simple yet physical and can be used in device simulations, or to characterize graphene on other substrates near room temperature and at high fields. We acknowledge financial support from the NRI, ONR, NSF, and valuable discussions with S. Datta, M. Fuhrer and E. Tutuc.

REFERENCES

- ¹ A. K. Geim, *Science* **324**, 1530 (2009).
- ² E. Pop, *Nano Research* **3**, 147 (2010).
- ³ S.V. Morozov, K.S. Novoselov, M.I. Katsnelson, F. Schedin, D.C. Elias, J.A. Jaszczak, and A.K. Geim, *Phys. Rev. Lett.* **100**, 016602 (2008); C. Jang, S. Adam, J. H. Chen, E. D. Williams, S. Das Sarma, and M. S. Fuhrer, *Physical Review Letters* **101**, 146805 (2008); Y. W. Tan, Y. Zhang, K. Bolotin, Y. Zhao, S. Adam, E. H. Hwang, S. Das Sarma, H. L. Stormer, and P. Kim, *Physical Review Letters* **99**, 246803 (2007).
- ⁴ M.-H. Bae, Z.-Y. Ong, D. Estrada, and E. Pop, in *9th IEEE Conf. Nanotechnology* (Genoa, Italy, 2009), pp. 818; M.-H. Bae, Z.-Y. Ong, D. Estrada, and E. Pop, <http://arxiv.org/abs/1004.0287> (2010).
- ⁵ Please see included supplementary materials and discussion.
- ⁶ T. Fang, A. Konar, H. L. Xing, and D. Jena, *Applied Physics Letters* **91**, 092109 (2007).
- ⁷ W. J. Zhu, V. Perebeinos, M. Freitag, and P. Avouris, *Physical Review B* **80**, 235402 (2009).
- ⁸ J. Martin, N. Akerman, G. Ulbricht, T. Lohmann, J. H. Smet, K. von Klitzing, and A. Yacoby, *Nature Physics* **4**, 144 (2008); Y. Zhang, V.W. Brar, C. Girit, A. Zettl, and M.F. Crommie, *Nature Physics* **5**, 722 (2009).
- ⁹ A. Deshpande, W. Bao, F. Miao, C. N. Lau, and B. J. LeRoy, *Phys. Rev. B* **79**, 205411 (2009).

- ¹⁰ S. Adam, E. H. Hwang, V. M. Galitski, and S. Das Sarma, *Proceedings of the National Academy of Sciences of the United States of America* **104**, 18392 (2007).
- ¹¹ I. Meric, M. Y. Han, A. F. Young, B. Ozyilmaz, P. Kim, and K. L. Shepard, *Nature Nanotechnology* **3**, 654 (2008).
- ¹² Hall mobility measurements yield identical results over the carrier density regime discussed here ($n > 6 \times 10^{11} \text{ cm}^{-2}$), as shown by Ponomarenko et al, *Phys. Rev. Lett.* **102**, 206603 (2009).
- ¹³ Z. Chen, W. Jang, W. Bao, C. N. Lau, and C. Dames, *Appl. Phys. Lett.* **95**, 161910 (2009).
- ¹⁴ Sample heating much beyond $\Delta T \sim 200 \text{ K}$ can also lead to unreproducible behavior (e.g. V_0 shift) due to thermal stress.
- ¹⁵ A. Barreiro, M. Lazzeri, J. Moser, F. Mauri, and A. Bachtold, *Phys. Rev. Lett.* **103**, 076601 (2009); J. Chauhan and J. Guo, *Appl. Phys. Lett.* **95**, 023120 (2009).
- ¹⁶ Eq. (6) is valid at carrier densities $n > (\omega_{OP}/v_F)^2/(2\pi) \approx 9.4 \times 10^{11} \text{ cm}^{-2}$ for $\hbar\omega_{OP} = 160 \text{ meV}$ and $1.1 \times 10^{11} \text{ cm}^{-2}$ for $\hbar\omega_{OP} = 55 \text{ meV}$, well within the range of the experiments here.
- ¹⁷ M. V. Fischetti, D. A. Neumayer, and E. A. Cartier, *J. Appl. Phys.* **90**, 4587 (2001).
- ¹⁸ K. M. Borysenko, J. T. Mullen, E. A. Barry, S. Paul, Y. G. Semenov, J. M. Zavada, M. Buongiorno Nardelli, and K. W. Kim, *Phys. Rev. B* **81** (12), 121412 (2010).
- ¹⁹ Y. Zhao, A. Liao, and E. Pop, *IEEE Electron Device Letters* **30**, 1078 (2009).
- ²⁰ C. Jacoboni, C. Canali, G. Ottaviani, and A. Alberigi Quaranta, *Solid-State Electronics* **20**, 77 (1977).
- ²¹ R. Quay, C. Moglestue, V. Palankovski, and S. Selberherr, *Materials Science in Semiconductor Processing* **3**, 149 (2000).

FIGURES

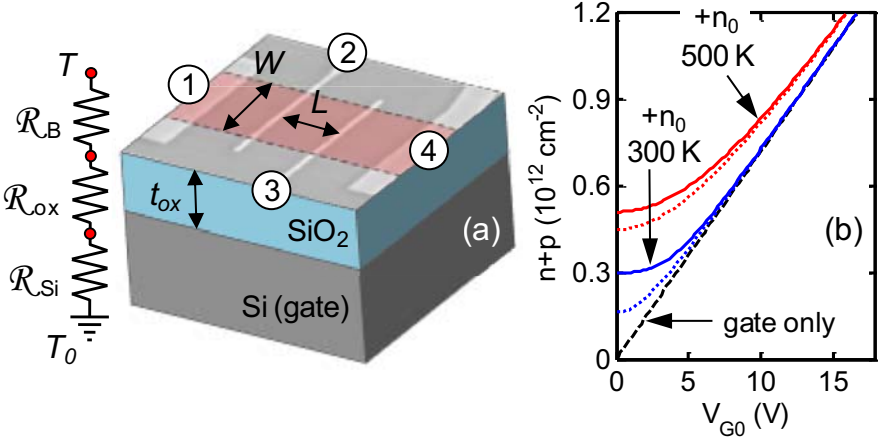


FIG. 1 (a) Schematic of graphene sample ($W = 7 \mu\text{m}$, $L = 4 \mu\text{m}$, $t_{ox} = 300 \text{ nm}$) connected to four-probe electrodes; graphene colorized for clarity. Thermal resistance model is used to calculate average temperature rise under high bias. **(b)** Calculated carrier density vs. gate voltage at 300 K (blue) and 500 K (red) in electron-doped regime ($n > p$). Solid lines include contribution from electrostatic inhomogeneity n^* and thermal carriers n_{th} (both relevant at 300 K), dotted lines include only n_{th} (dominant at 500 K). Black dashed line shows only contribution from gating, n_{cv} .

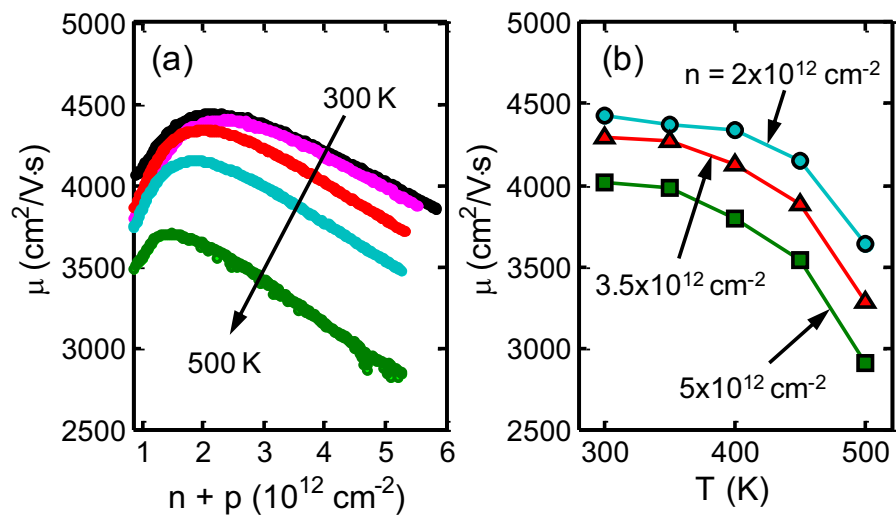


FIG. 2 (a) Mobility vs. carrier density in the electron-doped regime ($V_{G0} > 0$, $n > p$), obtained from conductivity measurements at $T = 300\text{--}500$ K, in 50 K intervals. The qualitative dependence on charge density is similar to that found in carbon nanotubes.¹⁹ (b) Mobility vs. temperature at $n = 2 \times 10^{12}$ (top), 3.5×10^{12} (middle), and $5 \times 10^{12} \text{ cm}^{-2}$ (bottom).

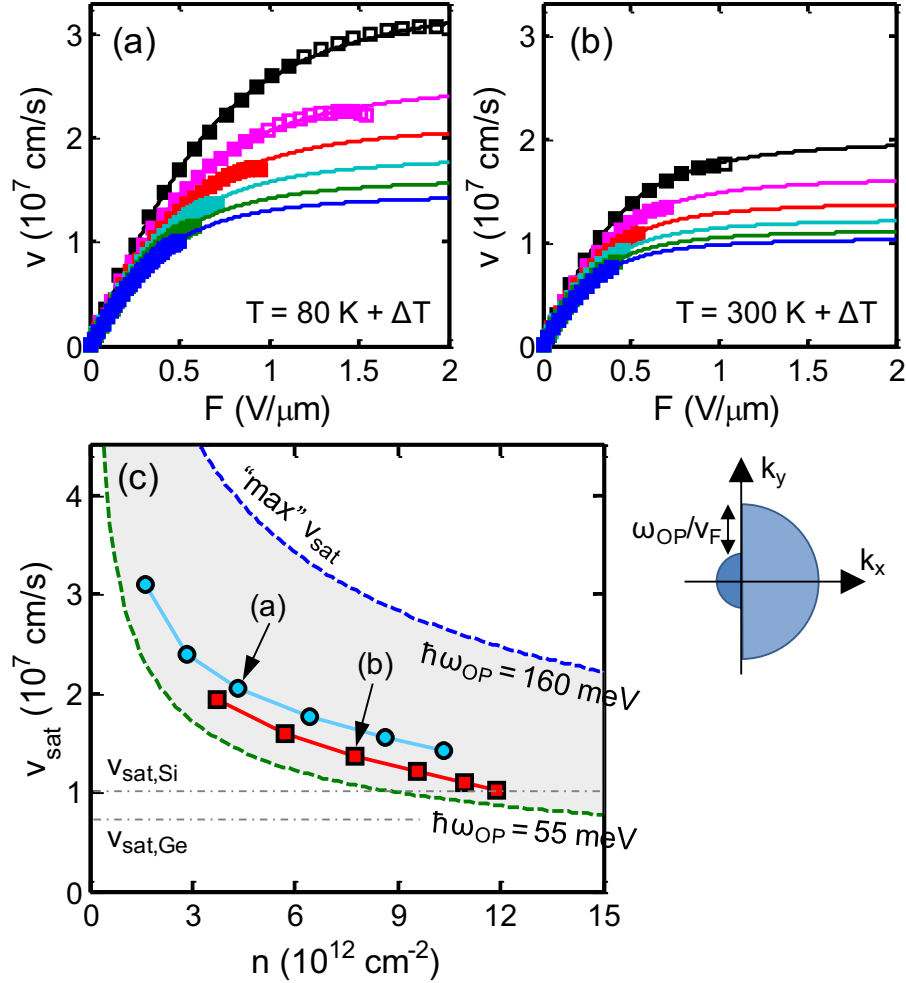


FIG. 3 Electron saturation velocity vs. carrier density. **(a)** Background temperature $T_0 = 80 \text{ K}$ with $V_{G0} = 10.5\text{--}60.5 \text{ V}$, and **(b)** $T_0 = 300 \text{ K}$ with $V_{G0} = 23.5\text{--}73.5 \text{ V}$ (in 10 V steps from top to bottom). Squares (data), lines (empirical fits), open squares have $\Delta T > 200 \text{ K}$ from Joule heating and were not used for fit. Changing fitting criteria to $\Delta T = 200 \pm 100 \text{ K}$ results in $< 8\%$ error. **(c)** Saturation velocity vs. electron density at $F = 2 \text{ V}/\mu\text{m}$. Side panel shows carrier distribution assumed for analytic model. Dashed lines show Eq. (6) with $\hbar\omega_{\text{OP}} = 55 \text{ meV}$ (SiO_2) and 160 meV (graphene). The latter also suggests the maximum intrinsic v_{sat} that could be achieved. Electron v_{sat} for Si and Ge are shown for comparison.^{20,21}

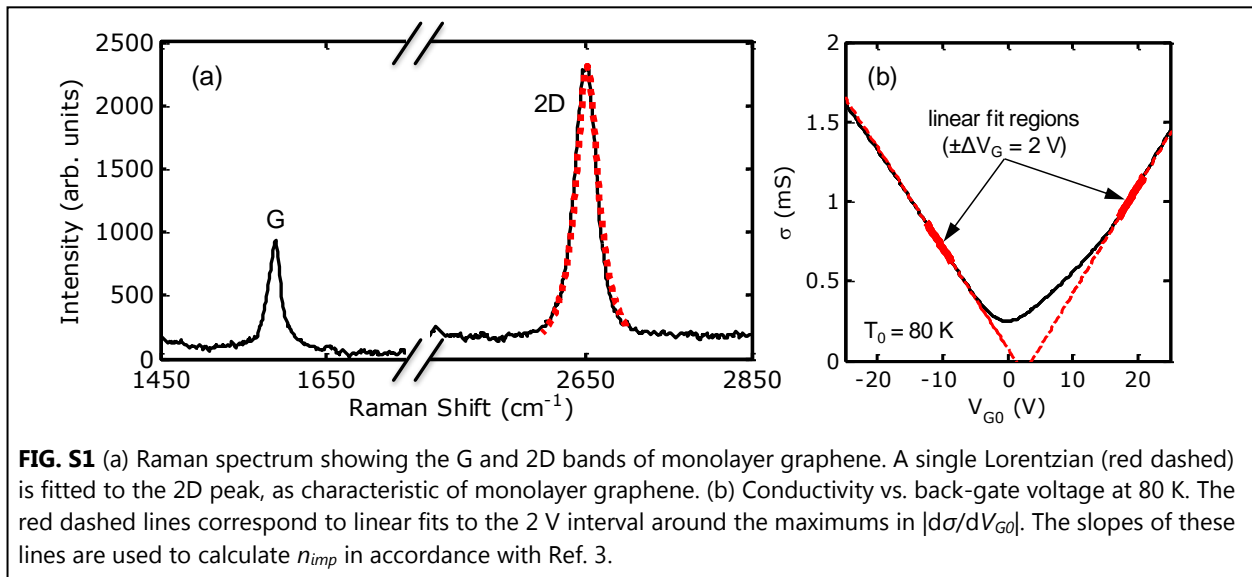
Supporting Online Materials for “Mobility and Saturation Velocity in Graphene on SiO₂” by V. E. Dorgan, M.-H. Bae, and E. Pop, University of Illinois, Urbana-Champaign, U.S.A.

1. Graphene Device Fabrication: We deposit graphene from mechanical exfoliation of natural graphite onto SiO₂ (dry thermally grown, thickness $t_{ox} = 300$ nm) with an n+ doped (2.5×10^{19} cm⁻³) Si substrate, which also serves as the back-gate (Fig. 1a). Electron beam lithography is used to define the four Cr/Pd (0.5/40 nm) electrodes, with inner voltage probes much narrower (~ 300 nm) than the graphene channel dimensions ($W = 7$ μ m, $L = 4$ μ m), to provide minimally invasive contacts. An additional lithography step followed by an oxygen plasma etch (75 W, 0.1 Torr for 15 s) creates the graphene channel.¹

2. Raman Spectroscopy: After device fabrication, Raman spectroscopy is used to confirm that the graphene flake is indeed monolayer graphene. The Raman 2D peak of monolayer graphene exhibits a single Lorentzian line shape.² In this study, Raman spectra were obtained using a Renishaw Raman spectrometer with a 633 nm laser excitation (power at the object: 10 mW) and a 50 \times in-air objective. Figure S1a shows the Raman spectrum obtained from the fabricated graphene device shown in Fig. 1a. The single Lorentzian fit to the 2D peak in Fig. S1 confirms that this sample is monolayer graphene, as does the approximate ratio (1:2) of the G to 2D peaks.

3. Extracting Impurity Density: The charged impurity density at the SiO₂ surface is determined based on the approach discussed in Ref. 3 and given by $n_{imp} = BC_{ox}|d\sigma/dV_{G0}|^{-1}$ where $B = 5 \times 10^{15}$ cm⁻² is a constant determined by the screened Coulomb potential in the random phase approximation (RPA)⁴ and $d\sigma/dV_{G0}$ is the slope of the low-field conductivity $\sigma = (L/W)(I_{14}/V_{23})$.

The slope is determined by a linear fit to σ over a $\Delta V_{G0} = 2$ V interval around the maximum of $|d\sigma/dV_{G0}|$ as shown in Fig. S1b. The value of n_{imp} used here is based on a conductivity measurement at 80 K, where mobility is limited by Coulomb scattering.⁵ From Eq. (10) of Ref. 6, we determine $n^* \approx 0.297n_{imp} \approx 2.63 \times 10^{11}$ cm⁻² in our sample (averaged over the electron- and hole-doped regimes), where n^* is the residual carrier puddle density representing the width of the minimum conductivity plateau. From n^* , we obtain $\Delta \approx \hbar v_F(\pi n^*)^{1/2} \approx 59$ meV and $\Delta V_0 \approx qn^*/C_{ox} \approx 3.66$ V in order to model the spatially inhomogeneous electrostatic potential (main text).



4. Hole Mobility and Uncertainty: As in the main text, the mobility for the hole-doped regime ($V_{G0} < 0$) is obtained and shown in Fig. S2a. Given the symmetric energy bands in graphene, the hole mobility here is similar to the electron mobility from Fig. 2a. Only one discrepancy exists for the 300 K data set, which does not show the typical mobility peak vs. carrier density as in all other measurements. This is most likely due to the calculated hole density underestimating the actual value in the device, probably due to a spatial inhomogeneity of the “puddle” regime that is not accurately predicted by the simple $\pm\Delta V_0$ potential model. We note the mobility shape recovers at higher temperatures (350-500 K), as thermal smearing washes out such inhomogeneities.

To understand additional uncertainty associated with this method, Ref. 6 noted that for the extracted n_{imp} the predicted plateau width is expected to be correct within a factor of two. This leads to uncertainty in determining ΔV_0 , and thus uncertainty in the charge density and extracted mobility values. However, this uncertainty is only notable around the Dirac point, where the potential ripple contributes to the total carrier density. This limits the “confidence region” in Figs. 2a and S2a, with charge density shown only $> 0.85 \times 10^{12} \text{ cm}^{-2}$. In Fig. S2b we estimate the mobility uncertainty at lower charge densities around the Dirac point, such that the upper and lower bounds result from a potential ripple of $\Delta V_0/2$ and $2\Delta V_0$ respectively.

5. Temperature Dependence of Thermal Resistance: Self-heating during high-field measurements is determined by Eq. (4), which raises the temperature of the graphene device and of the underlying SiO_2 as a function of input power during the measurement. The thermal resistance \mathcal{R}_{th} depends on temperature through κ_{ox} (thermal conductivity of SiO_2) and κ_{Si} (thermal conductivity of the doped Si wafer). These can be written as $\kappa_{ox} = \ln(T_{ox}^{0.52}) - 1.687$ and $\kappa_{Si} = 2.4 \times 10^4 / T_0$ by simple fitting to the experimental data in Refs. 7 and 8 respectively. Based on the thermal resistance model, we estimate the average oxide temperature as $T_{ox} = (T_0 + T)/2$ and the temperature of the silicon substrate as the background temperature T_0 . This allows a simple iterative method for calculating the graphene temperature rise (ΔT) during measurements.

6. Electrostatics in the High-Field Regime: During high-field measurements, the carrier density and temperature can vary across the device.⁹ As mentioned in the main text, we minimize this effect by carefully avoiding ambipolar transport and generally restricting our samples to average carrier density $> 2 \times 10^{12} \text{ cm}^{-2}$ at high fields. In addition, here we follow Ref. 9 to fully model this regime as shown in Fig. S3. Based on these simulation results, we confirm that it is valid to assume a constant (average) electric field and relatively uniform charge density across the active

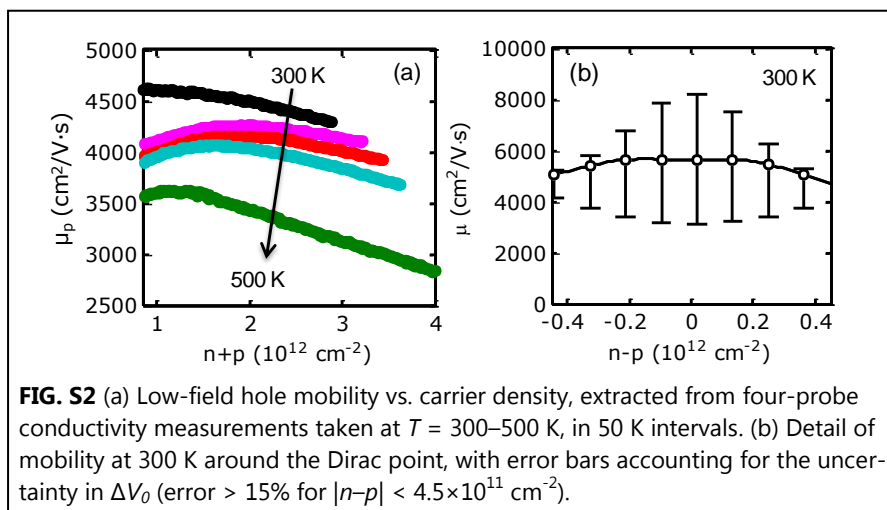
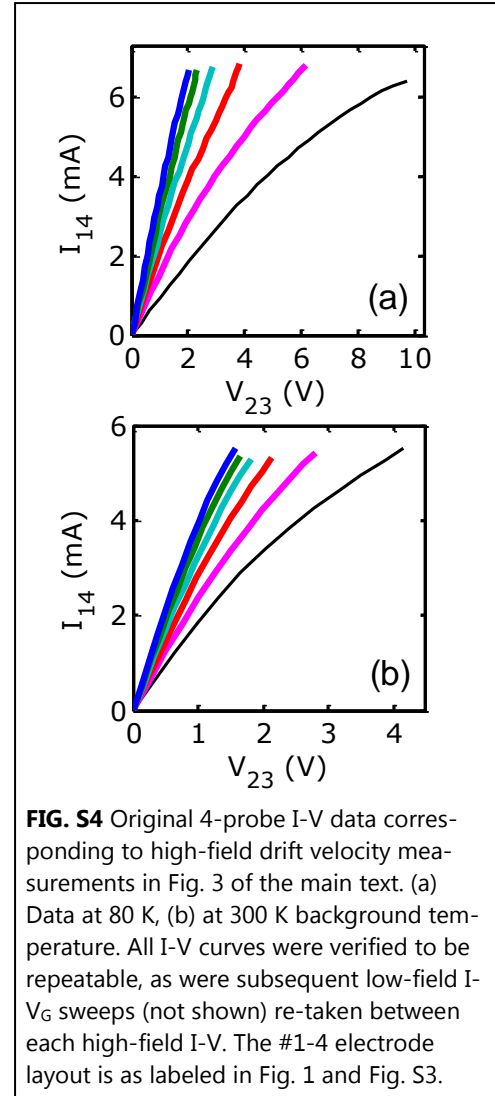
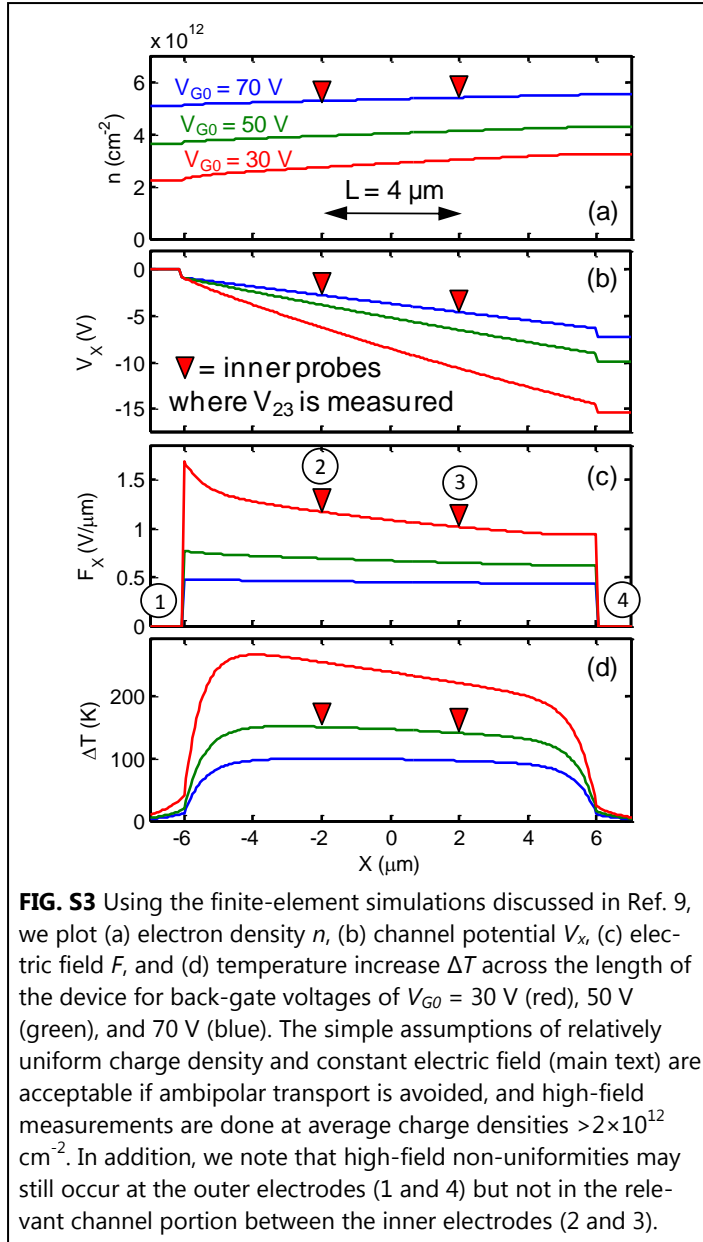


FIG. S2 (a) Low-field hole mobility vs. carrier density, extracted from four-probe conductivity measurements taken at $T = 300\text{--}500 \text{ K}$, in 50 K intervals. (b) Detail of mobility at 300 K around the Dirac point, with error bars accounting for the uncertainty in ΔV_0 (error $> 15\%$ for $|n-p| < 4.5 \times 10^{11} \text{ cm}^{-2}$).

region of the device between the inner electrodes, if the biasing scheme mentioned above is followed. The average carrier density in the channel is simply given by the average of the densities at electrodes 2 and 3 (as labeled in Fig. 1a), while the average field is $F = (V_2 - V_3)/L$.



REFERENCES

- ¹ B. Ozyilmaz, P. Jarillo-Herrero, D. Efetov, and P. Kim, *Applied Physics Letters* **91**, 192107 (2007).
- ² L. M. Malard, J. Nilsson, D. C. Elias, J. C. Brant, F. Plentz, E. S. Alves, A. H. Castro, and M. A. Pimenta, *Physical Review B* **76**, 201401 (2007).
- ³ J. H. Chen, C. Jang, S. Adam, M. S. Fuhrer, E. D. Williams, and M. Ishigami, *Nature Physics* **4**, 377 (2008).
- ⁴ E. H. Hwang, S. Adam, and S. Das Sarma, *Physical Review Letters* **98**, 186806 (2007).
- ⁵ J. H. Chen, C. Jang, S. D. Xiao, M. Ishigami, and M. S. Fuhrer, *Nature Nanotechnology* **3**, 206 (2008).
- ⁶ S. Adam, E. H. Hwang, V. M. Galitski, and S. Das Sarma, *Proceedings of the National Academy of Sciences of the United States of America* **104**, 18392 (2007).
- ⁷ S. M. Lee and D. G. Cahill, *Journal of Applied Physics* **81**, 2590 (1997).
- ⁸ M. Asheghi, K. Kurabayashi, R. Kasnavi, and K. E. Goodson, *Journal of Applied Physics* **91**, 5079 (2002).
- ⁹ M.-H. Bae, Z.-Y. Ong, D. Estrada, and E. Pop, in *9th IEEE Conf. Nanotechnology* (Genoa, Italy, 2009), pp. 818; M.-H. Bae, Z.-Y. Ong, D. Estrada, and E. Pop, <http://arxiv.org/abs/1004.0287> (2010).